

Unique Decay Modes and Signatures of pNGB scalars in $SU(5)/SO(5)$ Composite Higgs Model

^aNilanjana Kumar¹, ^bVandana Sahdev²

^a*Centre for Cosmology and Science Popularization (CCSP), SGT University, Gurugram, Haryana 122505, India*

^b*Department of Physics and Astrophysics, University of Delhi, Delhi-110007, India*

Abstract

The nature of the Higgs boson, whether it is elementary or composite, will be investigated through precision measurements in ongoing experiments. In composite Higgs scenarios, the Higgs may manifest as a pseudo Nambu-Goldstone boson (pNGB) arising from a strongly interacting sector. The $SU(5)/SO(5)$ Composite Higgs Model features a rich scalar sector, with the decay patterns of the scalars being heavily influenced by how fermions are embedded in various representations of $SU(5)$. We discuss how the mass of the pNGB scalars and their couplings depend functionally on the compositeness scale and parameters of the strong sector. Unique decay modes of the scalars emerge from the model when the mixing between the mass and the gauge eigenstates is non-negligible. We present a comprehensive and thorough analysis of the fermiophilic and fermiophobic decay modes of the pNGB scalars. One of our main findings is that the decay patterns of the two singly charged scalars differ significantly. Additionally, one pNGB scalar decays to another on-shell pNGB scalar when the masses are more than ~ 1 TeV. Both these factors play a significant role in creating highly distinctive signatures in collider experiments. A muon collider presents a promising avenue for detecting pNGB scalars with masses greater than 1 TeV, particularly, in final states involving multiple jets.

1 Introduction

The last missing piece of the Standard Model (SM), the Higgs boson, was discovered by ATLAS [1] and CMS [2] at the Large Hadron Collider (LHC) in 2012 and properties of the SM have been observed with great precision at the LHC so far, with hints of disagreement in some measurements [3–5]. Nevertheless, the question of whether the Higgs is a fundamental particle or composite, persists. Moreover, in the Standard Model, the Higgs mass is not protected by any symmetry, thus, it receives large corrections at higher scales. Also, SM does not provide any dynamical explanation to the mechanism of electroweak symmetry breaking (EWSB). Composite Higgs models [6–9] offer an elegant solution to the hierarchy problem of Higgs physics by predicting a new strongly interacting sector around TeV energy scale. In these models, Higgs emerges as a pseudo-Nambu Goldstone boson of the strong sector [6]. The global symmetry is spontaneously broken, protecting the Higgs mass from corrections above the compositeness scale (f). The angle of vacuum misalignment (θ) is expressed as $\sin \theta = v/f$, where $v = 246$ GeV, is the electroweak vacuum expectation value (v.e.v).

The minimal case, which is known as the Minimal Composite Higgs model, based on $SO(5)/SO(4)$ [10–12] predicts only one pNGB scalar. Depending upon the Global symmetry, the non-minimal scenarios predict new composite pNGB scalars. The popular non-minimal composite Higgs Scenarios are $SU(4)/Sp(4)$ [13], $SO(6)/SO(5)$ [14, 15], $SU(4)^2/SU(4)$ [16] etc. These models not only offer a very rich scalar spectrum, they also predict many observations such as flavor changing neutral

¹nilanjana.kumar@gmail.com

²vandanasahdev20@gmail.com

currents [16], dark matter [17], baryon asymmetry in the universe [18], anomalous magnetic moment measurements [19] etc. Moreover, these scalars exhibit unique decay modes. Thus, the signatures of these pNGB scalars may or may not match with the standard searches of the exotic scalars performed by the LHC [20, 21].

We choose to study a specific model $SU(5)/SO(5)$ [7, 22, 23] which exhibits a very rich scalar sector. Here, in addition to a scalar doublet, the other fields include one gauge singlet pseudo-scalar and three $SU(2)_L$ triplets. At low energy, this model looks similar to the Georgi Machacek Model [24, 25] with an additional singlet [26]. The composite sector and the SM fermion sector are coupled via a linear mixing between SM fermions and composite spin 1/2 operators under the Partial Compositeness framework [27], which requires the existence of heavy fermionic resonances [28]. Depending upon the embedding of SM fermions in the representations of $SU(5)$, the scalars may or may not have couplings with the fermions. This has been extensively studied in Ref: [22, 27]. For example, if the left-handed and right-handed fermions are in the adjoint representation of $SU(5)$, the coupling of the pNGB's to SM fermions vanishes, except with SM Higgs. It is shown in Ref: [22] that in other possible representations, the couplings of the pNGB scalars to the SM fermions can be generated. Hence, depending upon the embedding of the fermions, the decays of the pNGB scalars are very distinct: either *fermiophilic* or *fermiophobic*.

Recently, Ref: [21, 29] have studied a subset of the *fermiophilic* and *fermiophobic* scenarios in detail and discussed possible collider signatures and bounds from the LHC. The discussion in these papers are based on a simplified scenario where the value of the compositeness scale, f , and the masses of the scalars (hence, the mass differences among the pNGB scalars) are fixed at certain values. However, the value of the compositeness scale is generally fixed by the allowed fine tuning (measured in terms of the parameter $\xi = v^2/f^2$) in the model, which, depends heavily on the embedding of the fermions in different representations [30]. Although the value of f is constrained from the electroweak precision data, it is safe to take the range of the compositeness scale from 1 TeV to 5 TeV [22]. We explicitly calculate the masses of the pNGB scalars as functions of f and C_g , where, C_g is the contribution of the gauge loops in the pNGB potential and it encodes the dynamics of the strong sector. C_g is also influenced by the selected representation in the model being analyzed. The effect of these two parameters shows up in the branching ratios of the pNGB scalars that we study and some unique decay patterns of the scalars are identified.

In the previous studies of the pNGB scalars, the effect of mixing between the gauge and mass eigenstates of the scalars has been neglected. Here, we calculate the mass eigenstates and the couplings of pNGB scalars in terms of the mixing angles in the charged and the neutral sector. This mixing dictates the decay patterns of the pNGB scalars, which has not been studied earlier. In this work, we undertake the study of these interesting decay modes of the pNGB scalars. For a large value of f , say around 5 TeV, the pNGB scalars have masses of $\mathcal{O}(\text{TeV})$ and producing them at the LHC would be difficult, as found from the study of their production cross-sections. Although a high energy pp machine [31] may be a great option, the presence of abundant gauge bosons in the final state makes it challenging to observe these particles in multijet final states at the LHC due to the large QCD background. Given these limitations, the muon collider [32, 33] emerges as a promising alternative for detecting pNGB scalars with unique signatures.

2 Composite Higgs Model $SU(5)/SO(5)$

The non-minimal composite Higgs models deliver additional pNGB scalars, besides the standard Higgs doublet. The composite Higgs scenario based on the $SU(5)/SO(5)$ coset [22] leads to 14 pNGBs, all in all, which decompose under the custodial $SU(2)_L \times SU(2)_R$ as

$$14 \rightarrow (3, 3) + (2, 2) + (1, 1), \quad (1)$$

i.e., it includes a bi-triplet, the Higgs bi-doublet (H) and a singlet (η). The bi-triplet, further, decomposes as

$$(3, 3) \rightarrow 5 + 3 + 1, \quad (2)$$

which includes a quintuplet $\eta_5 \equiv (\eta_5^0, \eta_5^\pm, \eta_5^{\pm\pm})$, a triplet $\eta_3 \equiv (\eta_3^0, \eta_3^\pm)$ and a singlet η_1^0 of custodial $SU(2)_C$.

First we consider a particular scenario of the $SU(5)/SO(5)$ composite Higgs model in which the left- and right-handed fermions are embedded in the adjoint representation of $SU(5)$. In such a case, the coupling of the pNGB scalars (other than the SM Higgs) to SM fermions is forbidden. This situation is often termed as a *fermiophobic* scenario. On the other hand, their coupling to SM gauge bosons results from their covariant derivative which can be expressed through the lagrangian as

$$\begin{aligned} \mathcal{L}_{\Phi\Phi V} = & \frac{ie}{s_W} W^{-\mu} \sum_{i,j} \left[\kappa_W^{\phi_i^0 \phi_j^+} \phi_i^0 \overleftrightarrow{\partial}_\mu \phi_j^+ + \kappa_W^{\phi_i^- \phi_j^{++}} \phi_i^- \overleftrightarrow{\partial}_\mu \phi_j^{++} \right] + \text{h.c.} \\ & + \frac{ie}{s_W c_W} Z^\mu \left[\sum_{i < j} \kappa_Z^{\phi_i^0 \phi_j^0} \phi_i^0 \overleftrightarrow{\partial}_\mu \phi_j^0 + \sum_{i,j} \left(\kappa_Z^{\phi_i^+ \phi_j^-} \phi_i^+ \overleftrightarrow{\partial}_\mu \phi_j^- + \kappa_Z^{\phi_i^{++} \phi_j^{--}} \phi_i^{++} \overleftrightarrow{\partial}_\mu \phi_j^{--} \right) \right] \\ & - ie A^\mu \sum_i \left[\phi_i^+ \overleftrightarrow{\partial}_\mu \phi_i^- + 2\phi_i^{++} \overleftrightarrow{\partial}_\mu \phi_i^{--} \right]. \end{aligned} \quad (3)$$

In above equation, $\phi^0 = \{\eta, \eta_1^0, \eta_3^0, \eta_5^0\}$, $\phi^\pm = \{\eta_3^\pm, \eta_5^\pm\}$ and $\phi^{\pm\pm} = \eta_5^{\pm\pm}$. When only the Higgs doublet acquires a vacuum expectation value (v), the neutral scalars can evade all the constraints from LEP collider experiments and there are no corrections to the tree-level ρ -parameter [22, 27]. However, in these models, we also encounter additional gauge bosons. After integrating them out, one can derive the couplings of the pseudo-Nambu-Goldstone bosons (pNGBs) with the Standard Model gauge bosons through a dimension-5 term such as:

$$\begin{aligned} \mathcal{L}_{\Phi V \tilde{V}} = & \frac{e^2}{16\pi^2 v} \left[\phi^0 \left(\kappa_{\gamma\gamma}^{\phi^0} F_{\mu\nu} \tilde{F}^{\mu\nu} + \frac{2}{s_W c_W} \kappa_{\gamma Z}^{\phi^0} F_{\mu\nu} \tilde{Z}^{\mu\nu} + \frac{1}{s_W^2 c_W^2} \kappa_{ZZ}^{\phi^0} Z_{\mu\nu} \tilde{Z}^{\mu\nu} \right. \right. \\ & \left. \left. + \frac{2}{s_W^2} \kappa_{WW}^{\phi^0} W_{\mu\nu}^+ \tilde{W}^{-\mu\nu} \right) + \sum_i \phi^+ \left(\frac{2}{s_W} \kappa_{\gamma W}^{\phi^+} F_{\mu\nu} \tilde{W}^{-\mu\nu} + \frac{2}{s_W^2 c_W} \kappa_{ZW}^{\phi^+} Z_{\mu\nu} \tilde{W}^{-\mu\nu} \right) + \text{h.c.} \right. \\ & \left. + \frac{1}{s_W^2} \sum_i \phi^{++} \kappa_{W^- W^-}^{\phi^{++}} W_{\mu\nu}^- \tilde{W}^{-\mu\nu} + \text{h.c.} \right]. \end{aligned} \quad (4)$$

The Lagrangian involving the SM Higgs boson and EW gauge boson couplings can be written as,

$$\mathcal{L}_{hVV} = 2M_W^2 \frac{h}{v} \left[\kappa_{WW}^h W_\mu^+ W^{-\mu} + \kappa_{ZZ}^h \frac{1}{2c_W^2} Z_\mu Z^\mu \right]. \quad (5)$$

Hence, the complete *fermiophobic* Lagrangian is,

$$\mathcal{L}_{F-phobic} = \mathcal{L}_{\Phi\Phi V} + \mathcal{L}_{\Phi V \tilde{V}}. \quad (6)$$

If the fermions are in some other representation of $SU(5)$, as shown in [22], the coupling between the pNGB's and the SM fermions are generated. The interaction Lagrangian in the *fermiophilic* scenario can be written as,

$$\mathcal{L}_{F\text{-philic}} = \mathcal{L}_{\Phi\Phi V} + \mathcal{L}_{\Phi V\tilde{V}} + \mathcal{L}_{\Phi ff}. \quad (7)$$

where,

$$\mathcal{L}_{\Phi ff} = \phi^0 \left[\bar{t} \left(\kappa_t^{\Phi^0} + i\kappa_t^{\Phi^0} \gamma_5 \right) t + \bar{b} \left(\kappa_b^{\Phi^0} + i\tilde{\kappa}_b^{\Phi^0} \gamma_5 \right) b \right] + \Phi^+ \left[\kappa_{\bar{t}b,L}^{\phi^+} \bar{t} P_L b + (L \leftrightarrow R) \right] + \text{h.c.} \quad (8)$$

Here, coupling to only the third generation of the SM fermions is considered. Note that we assume there is no majorana type coupling with the leptons. Hence, decays of the pNGB scalars to the leptons are forbidden. In the next section, we discuss the gauge and fermionic couplings of the pNGB scalars, in detail.

3 Couplings of the Charged and Neutral pNGB Scalars

Let us discuss the masses and mixings of the pNGB's first. Being unmixed, the mass of the doubly charged scalar is obtained forthrightly as,

$$m_{\eta_5^{\pm\pm}}^2 = \frac{2}{3} m_h^2 \cot^2 2\theta + 4 \frac{C_g v^2}{s_\theta^2} (3g^2 + g'^2) + \frac{4}{3} \frac{C_g v^2}{s_\theta^2} (3 - c_{2\theta}) g'^2 \quad (9)$$

The mixing between the two singly charged custodial eigenstates, η_3^\pm and η_5^\pm , can be parameterized by the following mass matrix,

$$\mathcal{M}_\pm^2 = \begin{pmatrix} \frac{2}{3} m_h^2 \cot^2 2\theta + 4C_g(3g^2 + g'^2 - \frac{g'^2}{3} c_{2\theta}) \frac{v^2}{s_\theta^2} & 4C_g g'^2 \frac{v^2}{s_\theta^2} \\ 4C_g g'^2 \frac{v^2}{s_\theta^2} & \frac{2}{3} m_h^2 \cot^2 2\theta + 4C_g(3g^2 + \frac{g'^2}{2} + \frac{1}{6} g'^2 c_{2\theta}) \frac{v^2}{s_\theta^2} \end{pmatrix} \quad (10)$$

It should be noted that the scalars, η_3^\pm and η_5^\pm , are the gauge eigenstates. On diagonalisation, we obtain the mass eigenstates, which we denote as, η_1^\pm and η_2^\pm . The fields in the mass basis are related to the gauge basis via a rotation by an angle k_+ , given by,

$$\tan 2k_+ = \frac{2\mathcal{M}_{\pm 12}}{\mathcal{M}_{\pm 11} - \mathcal{M}_{\pm 22}}, \quad (11)$$

such that,

$$\eta_1^\pm = \cos k_+ \eta_3^\pm - \sin k_+ \eta_5^\pm \quad \eta_2^\pm = \sin k_+ \eta_3^\pm + \cos k_+ \eta_5^\pm. \quad (12)$$

The masses, $m_{\eta_1^\pm}^2$ and $m_{\eta_2^\pm}^2$ are obtained, straightforwardly, from the mass matrix \mathcal{M}_\pm^2 .

The neutral scalar, η_3^0 , being CP even, does not mix with other scalars. In addition, the other singlet scalar, η , mixes with η_1^0 and η_5^0 but the mixing is negligible. Hence, their masses are,

$$\begin{aligned} m_{\eta_3^0}^2 &\approx \frac{2}{3} m_h^2 \cot^2 2\theta + 4 \frac{C_g v^2}{\sin^2 \theta} \left((3g^2 + g'^2) + \frac{2}{3} g'^2 c_{2\theta} \right). \\ m_\eta^2 &\approx \frac{5}{6} \frac{m_h^2}{s_\theta^2} - \frac{20}{3} C_g (3g^2 + g'^2) \frac{v^2}{s_\theta^2}. \end{aligned} \quad (13)$$

On the other hand, there exists a significant mixing between η_1^0 and η_5^0 . The 2×2 mass matrix is,

$$\mathcal{M}^2 = \begin{pmatrix} \frac{1}{6} \frac{m_h^2}{s_\theta^2} + 4C_g(3g^2 + g'^2) \frac{v^2}{s_\theta^2} & \frac{8}{3} \sqrt{2} C_g g'^2 \frac{v^2}{s_\theta^2} \\ \frac{8}{3} \sqrt{2} C_g g'^2 \frac{v^2}{s_\theta^2} & \frac{1}{6} \frac{m_h^2}{s_\theta^2} + 4C_g(3g^2 + g'^2) \frac{v^2}{s_\theta^2} - \frac{8}{3} C_g g'^2 \frac{v^2}{s_\theta^2} \end{pmatrix}. \quad (14)$$

The mass eigenstates (η_1, η_2) are related to the gauge eigenstates (η_1^0, η_5^0) via a rotation by an angle, k_0 , given by,

$$\tan 2k_0 = \frac{2\mathcal{M}_{12}}{\mathcal{M}_{11} - \mathcal{M}_{22}}, \quad (15)$$

and the mass eigenstates are

$$\eta_1 = \cos k_0 \eta_1^0 - \sin k_0 \eta_5^0, \quad \eta_2 = \sin k_0 \eta_1^0 + \cos k_0 \eta_5^0. \quad (16)$$

It is straightforward to obtain the masses, $m_{\eta_1}^2$ and $m_{\eta_2}^2$, from the mass matrix, \mathcal{M}^2 . Having obtained the mass spectrum, we derive the couplings of the pNGB scalars in terms of the model parameters and express them in the mass basis. It is interesting to find that the effect of the mixing angles, k_0 and k_+ , is not always negligible. The *fermiophobic* couplings of the pNGB scalars are listed in Table:1 and Table:2. Note that the mixing angles in the charged and the neutral sector depend on the parameters C_g and f , as $\sin \theta \sim v/f$. We would like to emphasise that the previous studies have not considered the effect of these mixing angles in the couplings of pNGB. However, in the limit of small mixing angles, that is small k_+ and k_0 , we get back the expressions where the mass eigenstates are assumed to be the same as the gauge eigenstates. In the *fermiophilic* scenario, the coupling of

	η_1^+	η_2^+	η_5^{++}
η_3^0	$-\frac{i}{2} c_{k_+} - \frac{c_\theta}{2} s_{k_+}$	$-\frac{i}{2} s_{k_+} + \frac{c_\theta}{2} c_{k_+}$	
η_1	$\frac{c_\theta}{2\sqrt{3}} s_{k_0} c_{k_+} + \frac{i\sqrt{3}}{2} s_{k_0} s_{k_+} + \sqrt{\frac{2}{3}} c_\theta c_{k_0} c_{k_+}$	$\frac{c_\theta}{2\sqrt{3}} s_{k_0} s_{k_+} - \frac{i\sqrt{3}}{2} s_{k_0} c_{k_+} + \sqrt{\frac{2}{3}} c_\theta c_{k_0} s_{k_+}$	
η_2	$-\frac{c_\theta}{2\sqrt{3}} c_{k_0} c_{k_+} - \frac{i\sqrt{3}}{2} c_{k_0} s_{k_+} + \sqrt{\frac{2}{3}} c_\theta s_{k_0} c_{k_+}$	$-\frac{c_\theta}{2\sqrt{3}} c_{k_0} s_{k_+} + \frac{i\sqrt{3}}{2} c_{k_0} c_{k_+} + \sqrt{\frac{2}{3}} c_\theta s_{k_0} s_{k_+}$	
η_1^+			$\frac{c_\theta}{\sqrt{2}} c_{k_+} + \frac{i}{\sqrt{2}} s_{k_+}$
η_2^+			$\frac{c_\theta}{\sqrt{2}} s_{k_+} - \frac{i}{\sqrt{2}} c_{k_+}$

	η_1	η_2	η_1^-	η_2^-	η_5^{--}
η_3^0	$-\frac{ic_\theta}{\sqrt{3}} s_{k_0} + i\sqrt{\frac{2}{3}} c_\theta c_{k_0}$	$\frac{ic_\theta}{\sqrt{3}} c_{k_0} + i\sqrt{\frac{2}{3}} c_\theta s_{k_0}$			
η_1^+			$-\frac{c_{2W}}{2}$	$-\frac{ic_\theta}{2}$	
η_2^+			$\frac{ic_\theta}{2}$	$\frac{c_{2W}}{2} (c_{k_+}^2 - s_{k_+}^2)$	
η_5^{++}					$-c_{2W}$

Table 1: $\Phi\Phi V$ couplings in the mass basis of the pNGB scalars.

the pNGB scalars with the third generation SM quarks are parameterized as,

$$k_t^{\phi^0} = c_t \frac{m_t}{f}, \quad k_b^{\phi^0} = c_b \frac{m_b}{f}, \quad k_{tb}^{\phi^+} = c_{tb} \frac{m_t}{f}, \quad (17)$$

at the leading order. The exact values of c_t , c_b and c_{tb} depend on the details of the embedding. Without the loss of generality, we assume that these parameters are of $\mathcal{O}(1)$. These couplings become

	$\kappa_{\gamma\gamma}^{\phi^0}$	$\kappa_{\gamma Z}^{\phi^0}$	$\kappa_{ZZ}^{\phi^0}$	
η_1	$\frac{2s_\theta}{\sqrt{3}}s_{k_0} + \sqrt{\frac{2}{3}}s_\theta c_{k_0}$	$\frac{c_{2W}s_\theta}{\sqrt{3}}s_{k_0} + \frac{c_{2W}s_\theta}{\sqrt{6}}c_{k_0}$	$-\frac{(1-3c_{4W}+2c_{2\theta})s_\theta}{12\sqrt{3}}s_{k_0} + \frac{(1+6c_{4W}-7c_{2\theta})s_\theta}{24\sqrt{6}}c_{k_0}$	
η_2	$-\frac{2s_\theta}{\sqrt{3}}c_{k_0} + \sqrt{\frac{2}{3}}s_\theta s_{k_0}$	$-\frac{c_{2W}s_\theta}{\sqrt{3}}c_{k_0} + \frac{c_{2W}s_\theta}{\sqrt{6}}s_{k_0}$	$\frac{(1-3c_{4W}+2c_{2\theta})s_\theta}{12\sqrt{3}}c_{k_0} + \frac{(1+6c_{4W}-7c_{2\theta})s_\theta}{24\sqrt{6}}s_{k_0}$	
η	$\sqrt{\frac{2}{5}}s_\theta$	$-\frac{c_{2W}s_\theta}{\sqrt{10}}$	$\frac{(c_{4W}+3c_\theta^2)s_\theta}{4\sqrt{10}}$	
	$\kappa_{W+W-}^{\phi^0}$	$\kappa_{\gamma W-}^{\phi^+}$	$\kappa_{ZW-}^{\phi^+}$	$\kappa_{W-W-}^{\phi^{++}}$
η_1	$\frac{s_\theta^3}{6\sqrt{3}}s_{k_0} - \frac{7s_\theta^3}{12\sqrt{6}}c_{k_0}$			
η_2	$\frac{-s_\theta^3}{6\sqrt{3}}c_{k_0} - \frac{7s_\theta^3}{12\sqrt{6}}s_{k_0}$			
η	$-\frac{(3c_{2\theta}+5)s_\theta^2}{8\sqrt{10}}$			
η_1^+		$-\frac{s_{2\theta}}{4}c_{k_+} - \frac{is_{2\theta}}{2}s_{k_+}$	$\frac{s_W^2 s_{2\theta}}{4}c_{k_+} - \frac{i(c_{2W}-c_{2\theta}-2)s_\theta}{12}s_{k_+}$	
η_2^+		$-\frac{s_{2\theta}}{4}s_{k_+} + \frac{is_{2\theta}}{2}c_{k_+}$	$\frac{s_W^2 s_{2\theta}}{4}s_{k_+} + \frac{i(c_{2W}-c_{2\theta}-2)s_\theta}{12}c_{k_+}$	
η_5^{++}				$-\frac{s_\theta^3}{3\sqrt{2}}$

Table 2: $\Phi V\tilde{V}$ couplings in the mass basis of the pNGB scalars.

a function of the mixing angles k_+ and k_0 when pNGB scalars are in the mass eigenstates. In Table 3, we list the *fermiophilic* couplings in the mass basis for all pNGB scalars and show their approximate values at $f = 2.5$ TeV and 5 TeV. It is important to observe that the *fermiophilic* couplings diminish in strength when f is large, as evident from Table 3. Further, we observe that as a result of the

Coupling	Value	$f = 2.5$ TeV	$f = 5$ TeV
$k_{\bar{t}b}^{\eta_2^+}$	$c_{tb}(c_{k_+} + s_{k_+})\frac{m_t}{f}$	0.098	0.049
$k_{\bar{t}b}^{\eta_1^+}$	$c_{tb}(c_{k_+} - s_{k_+})\frac{m_t}{f}$	0.00017	0.000083
$k_t^{\eta_2}$	$c_t(c_{k_0} + s_{k_0})\frac{m_t}{f}$	0.096	0.048
$k_t^{\eta_1}$	$c_t(c_{k_0} - s_{k_0})\frac{m_t}{f}$	0.016	0.008
$k_b^{\eta_2}$	$c_b(c_{k_0} + s_{k_0})\frac{m_b}{f}$	0.002	0.001
$k_b^{\eta_1}$	$c_b(c_{k_0} - s_{k_0})\frac{m_b}{f}$	0.0004	0.0002
$k_b^{\eta_3^0}, k_b^\eta$	$c_b\frac{m_b}{f}$	0.0019	0.001
$k_t^{\eta_3^0}, k_t^\eta$	$c_t\frac{m_t}{f}$	0.069	0.034

Table 3: The *fermiophilic* couplings of the pNGB scalars in the mass basis at different f and for $c_t = c_b = c_{\bar{t}b} = 1$. The couplings for the conjugate fields have same values.

mixing, the coupling of η_1^+ to $\bar{t}b$ is exceptionally suppressed, in contrast to the coupling of η_2^+ to $\bar{t}b$. In comparison, for the neutral sector, the couplings of η_1 and η_2 to the SM quarks differ by only one order of magnitude. Hence, in the *fermiophilic* scenario, the decay modes of η_1^+ and η_2^+ are expected to be very different whereas the decay modes of η_1 and η_2 should not differ much, as we will discuss in the next section.

4 Decays of the pNGB Scalars

In the previous section, we demonstrated how the masses, mixings and couplings of the pNGB scalars are a function of the model parameters, C_g and f , where f is present through $\sin \theta = v/f$. The value of these model parameters leads to specific patterns of mixings and the mass splittings between the pNGB scalars which crucially affects the decay modes of these scalars. Reference [22] presented a comprehensive analysis of the mass differences among these pNGB scalars and explored how these differences are influenced by the value of C_g across all the possible representations. In Table:4, we show the mass spectrum at different benchmark values of the parameters, C_g and f . In Figure:1, we

Mass (GeV)	f=1 TeV		f=2.5 TeV		f=5 TeV	
	$C_g = 0.01$	$C_g = 0.02$	$C_g = 0.01$	$C_g = 0.02$	$C_g = 0.01$	$C_g = 0.02$
-						
η_1^\pm	286.3	358.7	743	918.4	1493.8	1843.1
η_2^\pm	310.6	397.1	801.7	1012.3	1610.6	2030.4
$\eta_5^{\pm\pm}$	307.4	392.1	793.5	999.3	1594.1	2004.1
η	349.5	171.8	873.7	429.5	1747.5	859
η_1	302.8	374.8	757	936.9	1514.1	1873.8
η_2	319.3	401.2	798.2	1003	1596.5	2005.9
η_3^0	306.4	390.5	793.1	998.7	1593.9	2003.8

Table 4: Mass of the pNGB scalars in GeV at different benchmark scenarios.

plot the mass differences between the scalars as a function of C_g (top panel), and, as a function of f (bottom panel). Here, we have chosen to represent only those mass differences which play a crucial role in the decay of the charged scalars. It is clear from both, Table:4 and Figure:1, that the masses and the mass differences are highly sensitive to the parameters, C_g and f , particularly f . Thus, while analysing the decay modes, fixing the masses at one certain value or assuming a fixed mass splitting, is not always correct. A more insightful approach for analyzing the decays of the scalars is to include the effect of various mixings and mass-splittings, which we discuss in the next subsection.

Before proceeding further, we reflect upon a few nuances. The singlet scalar, η , receives a negative mass correction from the gauge sector [22]. Hence, as shown in Table:4, as the value of C_g increases, the mass of η decreases. At a particular value of C_g , the singlet becomes tachyonic and this places an upper limit on C_g viz., $C_g < 0.023$. Hence, while observing the decay modes of the pNGB scalars, we vary C_g between 0.001 – 0.023. We also observe from Table:4 that the lowest mass scalar is either η or η_1 . We, now, describe the decay modes of the pNGB scalars, in detail.

4.1 Branching Ratios of $\eta_5^{\pm\pm}$

The branching ratios of the doubly charged scalar $\eta_5^{\pm\pm}$ are plotted in Figure:2, for the *fermiophobic* scenario (top panel) and the *fermiophilic* scenario (bottom panel). The masses are a function of C_g , and we choose three values of f viz., 1 TeV (left), 2.5 TeV (middle) and 5 TeV (right) which covers the range of pNGB masses from $\sim 200 - 2000$ GeV. From the mass-differences depicted in Figure:1, we see that the relation $m_{\eta_5^{\pm\pm}} > m_{\eta_1^\pm}$ is true for any value of C_g and f . On the other hand, the mass-splitting between $m_{\eta_5^{\pm\pm}}$ and $m_{\eta_2^\pm}$ is almost negligible. Hence, the doubly charged scalar preferentially decays to η_1^\pm . In the *fermiophobic* scenario *i.e.*, when couplings to fermions are absent, the dominating mode of decay, at smaller values of f *i.e.*, for the cases $f = 1$ TeV and 2.5 TeV here, is

$$\eta_5^{\pm\pm} \rightarrow W^{\pm*} \eta_1^\pm \rightarrow (q\bar{q}) \eta_1^\pm, (l\nu) \eta_1^\pm, \quad (18)$$

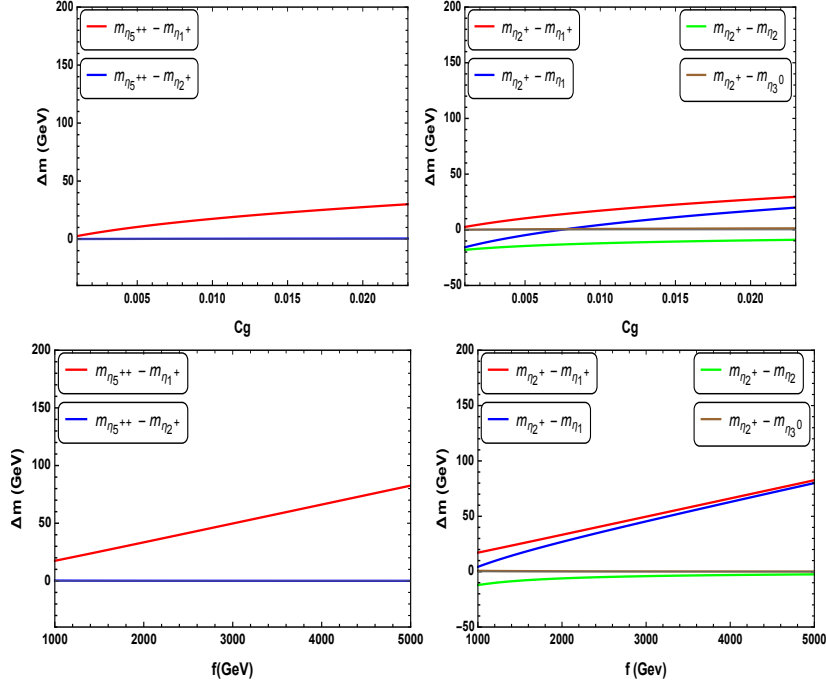


Figure 1: Mass difference among the scalar pNGB's as a function C_g with $f = 1$ TeV (Top) and as a function of f with $C_g = 0.01$ (Bottom).

where W^* is an off-shell W boson leading to the subsequent three body decays. At $f = 5$ TeV and $C_g \geq 0.01$, $\eta_5^{\pm\pm}$ becomes larger than 1.6 TeV and the mass difference between $\eta_5^{\pm\pm}$ and η_1^{\pm} becomes sufficient for the on-shell decay to the W boson,

$$\eta_5^{\pm\pm} \rightarrow W^{\pm}\eta_1^{\pm}. \quad (19)$$

The *fermiophobic* branching ratios for $\eta_5^{\pm\pm}$ are depicted in Figure:2 (top panel). The decays to η_1^{\pm} are shown by the curves in red: dashed (off-shell gauge boson) and solid (on-shell gauge boson).

In principle, the decay via off-shell scalar particle *i.e.*, $\eta_5^{\pm\pm} \rightarrow W^{\pm}\eta_i^{\pm*}$, $i = 1, 2$ is also possible, leading to three gauge bosons. However, the couplings of the pNGB scalars to the gauge bosons are suppressed in comparison to the couplings of the gauge bosons to quarks and leptons. For the same reason, the on-shell decay to two gauge bosons,

$$\eta_5^{\pm\pm} \rightarrow W^{\pm}W^{\pm}, \quad (20)$$

is suppressed.

As discussed before, the couplings of the pNGB scalars to the SM fermions are allowed in some particular representations. In such *fermiophilic* scenarios, three body decays of pNGB scalars via other off-shell scalars become prominent where the off-shell scalars decay to two SM fermions. Further, these decays are dominant over the three body decays via off-shell gauge bosons³.

The *fermiophilic* branching ratios for $\eta_5^{\pm\pm}$ are depicted in Figure:2 (bottom panel). The decay of $\eta_5^{\pm\pm}$ to the gauge bosons are suppressed as before. At $f = 1$ TeV, for smaller masses, decay via off shell

³The three-body decays where off-shell scalars decay to gauge bosons were suppressed because the coupling to the SM gauge bosons occurs via dimension-5 terms. On the other hand, coupling to the fermions are at tree level and hence not suppressed.

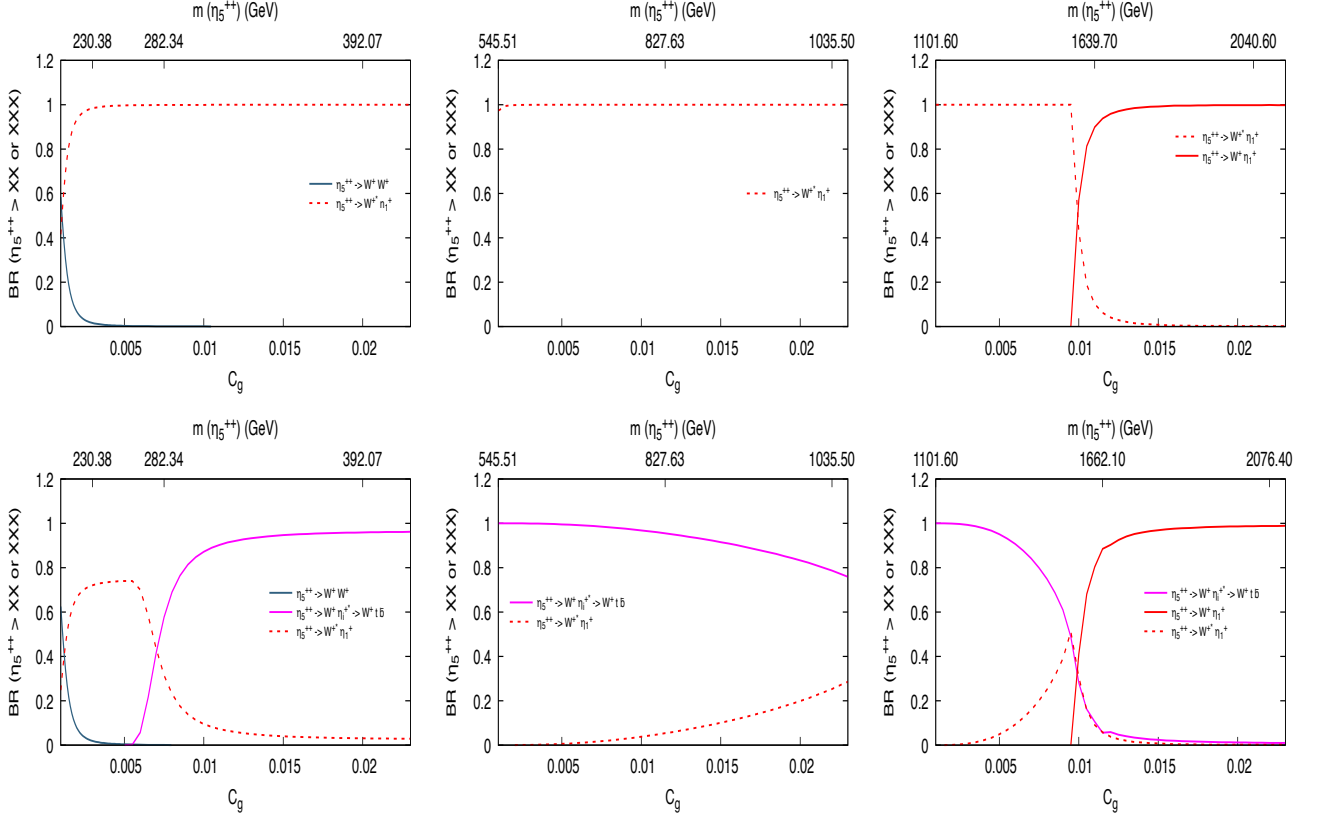


Figure 2: Branching ratios of $\eta_5^{\pm\pm}$ for the fermiophobic scenario (top panel) and the *fermiophilic* scenario (bottom panel) at $f : 1$ TeV (left), 2.5 TeV (middle) and 5 TeV (right).

W boson dominates, leading to the following final states.

$$\eta_5^{\pm\pm} \rightarrow W^{\pm*} \eta_1^{\pm} \rightarrow (q\bar{q})\eta_1^{\pm}, (l\nu)\eta_1^{\pm}. \quad (21)$$

With increase in mass, the decays of $\eta_5^{\pm\pm}$ proceed via off-shell $\eta_{1,2}^{\pm}$, leading to the three body final state,⁴

$$\eta_5^{\pm\pm} \rightarrow W^{\pm} \eta_i^{\pm*} \rightarrow W^{\pm} t\bar{b}. \quad (22)$$

At $f = 2.5$ TeV, the same decay mode dominates. However, with increasing f , the branching ratio of the pNGB scalars to the fermions gets smaller since the *fermiophilic* coupling is proportional to m_t/f . Hence, at larger masses, when $f = 5$ TeV and $C_g \geq 0.01$, decay to on shell W and on shell η_1^{\pm} dominates,

$$\eta_5^{\pm\pm} \rightarrow W^{\pm} \eta_1^{\pm}. \quad (23)$$

4.2 Branching Ratios of η_2^{\pm}

The branching ratios of the singly charged pNGB scalar η_2^{\pm} are plotted in Figure:3, for the *fermiophobic* scenario (top panel) and the *fermiophilic* scenario (bottom panel). The various parameters are the same as before. First, we, discuss the *fermiophobic* case. The main decay channels of η_2^{\pm} upto $f = 2.5$

⁴Here, in the writing, we have used the redefinition $t = t, \bar{t}, b = b, \bar{b}, q = q, \bar{q}$ and $l = l^+, l^-$, where particle and antiparticle are summed over.

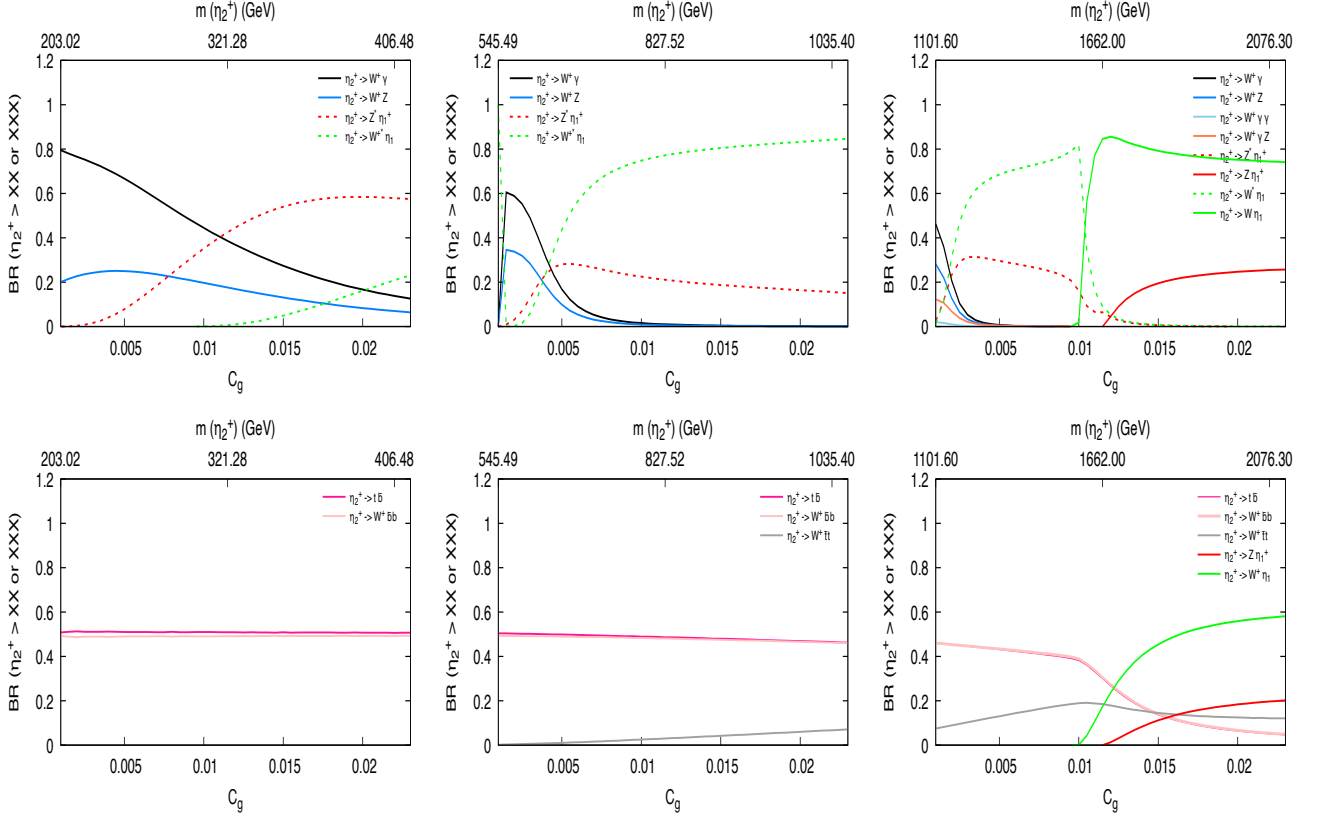


Figure 3: Branching ratios of η_2^\pm for the *fermiophobic* scenario (top panel) and the *fermiophilic* scenario (bottom panel) at $f : 1$ TeV (left), 2.5 TeV (middle) and 5 TeV (right).

TeV are,

$$\eta_2^\pm \rightarrow W^\pm Z, W^\pm \gamma, \quad (24)$$

$$\eta_2^\pm \rightarrow Z^* \eta_1^\pm \rightarrow (ll)\eta_1^\pm, (q\bar{q})\eta_1^\pm, \quad (25)$$

$$\eta_2^\pm \rightarrow W^{\pm*} \eta_1 \rightarrow (l\nu)\eta_1, (q\bar{q})\eta_1. \quad (26)$$

At small masses, the insufficient mass-splitting with other pNGB scalars leads to $W^\pm \gamma$ being the dominant decay mode. As the mass increases, decays to lighter scalars become possible via off-shell gauge bosons *viz.*, $Z^* \eta_1^\pm$ and $W^{\pm*} \eta_1$ and these start to dominate. This is shown in Figure:3 (top left and middle). Also, with increase in f , the coupling to η_1 dominates over the coupling to η_1^\pm , as shown by the red and green dashed curves in these figures. For $f = 5$ TeV (Figure:3, top right), however, the increased mass-splitting with lighter scalars facilitates decays of η_2^\pm to these scalars, accompanied with on-shell gauge bosons, W and Z *viz.*,

$$\eta_2^\pm \rightarrow Z \eta_1^\pm, \quad (27)$$

$$\eta_2^\pm \rightarrow W^\pm \eta_1. \quad (28)$$

Considering the mass-hierarchy, decay of η_2^\pm to any other pNGB scalar is not allowed.

We now discuss the *fermiophilic* decay modes of η_2^\pm , as shown in Figure:3 (bottom panel). At $f = 1$ TeV, following decays to SM fermions dominate *viz.*,

$$\eta_2^\pm \rightarrow tb, \quad (29)$$

$$\eta_2^\pm \rightarrow W^\pm \eta_i^* \rightarrow W^\pm bb, \quad (30)$$

$$\eta_2^\pm \rightarrow tb \rightarrow W^\pm bb, \quad (31)$$

where η_i^* is the sum over all the neutral scalars. Note that the contribution to the final state $W^\pm bb$ comes from both the processes, as listed above. It must be mentioned here that due to mixing, the coupling of η_2^\pm to SM fermions is enhanced compared to that of other scalars. Consequently, major contribution comes from the process with the SM quark as the mediator.

At $f = 2.5$ TeV, an additional decay channel opens up due to the increased mass *viz.*,

$$\eta_2^\pm \rightarrow W^\pm \eta_i^* \rightarrow W^\pm tt. \quad (32)$$

Because of the coupling $\eta_2^\pm tb$ being dominant (See Table:3), however, the branching ratios to tb and $W^\pm b\bar{b}$ are still larger. With further increase in f , however, the branching ratios to the fermions start to fall as the involved coupling is inversely proportional to f . Instead, the on-shell gauge bosons and pNGB scalars start to dominate *i.e.*,

$$\eta_2^\pm \rightarrow W^\pm \eta_1, \quad (33)$$

$$\eta_2^\pm \rightarrow Z \eta_1^\pm. \quad (34)$$

This is depicted for the case of $f = 5$ TeV (Figure:3, bottom right).

4.3 Branching Ratios of η_1^\pm

The branching ratios of η_1^\pm are very interesting as they differ from that of the other singly charged scalar, η_2^\pm . The graphs are plotted in Figure:4, for the *fermiophobic* scenario (top panel) and the *fermiophilic* scenario (bottom panel).

First, we discuss the *fermiophobic* scenario. From Table:4, we can observe that at lower values of C_g , η_1^\pm has the lowest mass in the spectrum and therefore, any on-shell decays involving other scalars are prohibited. At larger C_g , η_1^\pm is the second lightest pNGB scalar, next to the lightest, η . However, η does not couple to any other pNGB scalar. As a result, η_1^\pm cannot decay to an on-shell pNGB scalar, at all⁵. The decay modes dominant at smaller masses are,

$$\eta_1^\pm \rightarrow W^\pm Z, W^\pm \gamma, \quad (35)$$

as shown in Figure:4 (top left and middle). At larger masses, however, three body decays via off-shell pNGB scalars dominate *i.e.*,

$$\eta_1^\pm \rightarrow W^\pm \eta_i^*, \quad (36)$$

$$\eta_1^\pm \rightarrow W^\pm \eta_5^{\pm\pm*}, \quad (37)$$

$$\eta_1^\pm \rightarrow Z \eta_2^{\pm*}, \quad (38)$$

where $\eta_i = \eta_1, \eta_2$ or η_3^0 . These off-shell scalars finally decay to the gauge bosons leading to final states with three gauge bosons. Hence, we observe that in the *fermiophobic* case, the decay patterns of η_1^\pm and η_2^\pm are very different.

⁵This is unlike the case of η_2^\pm .

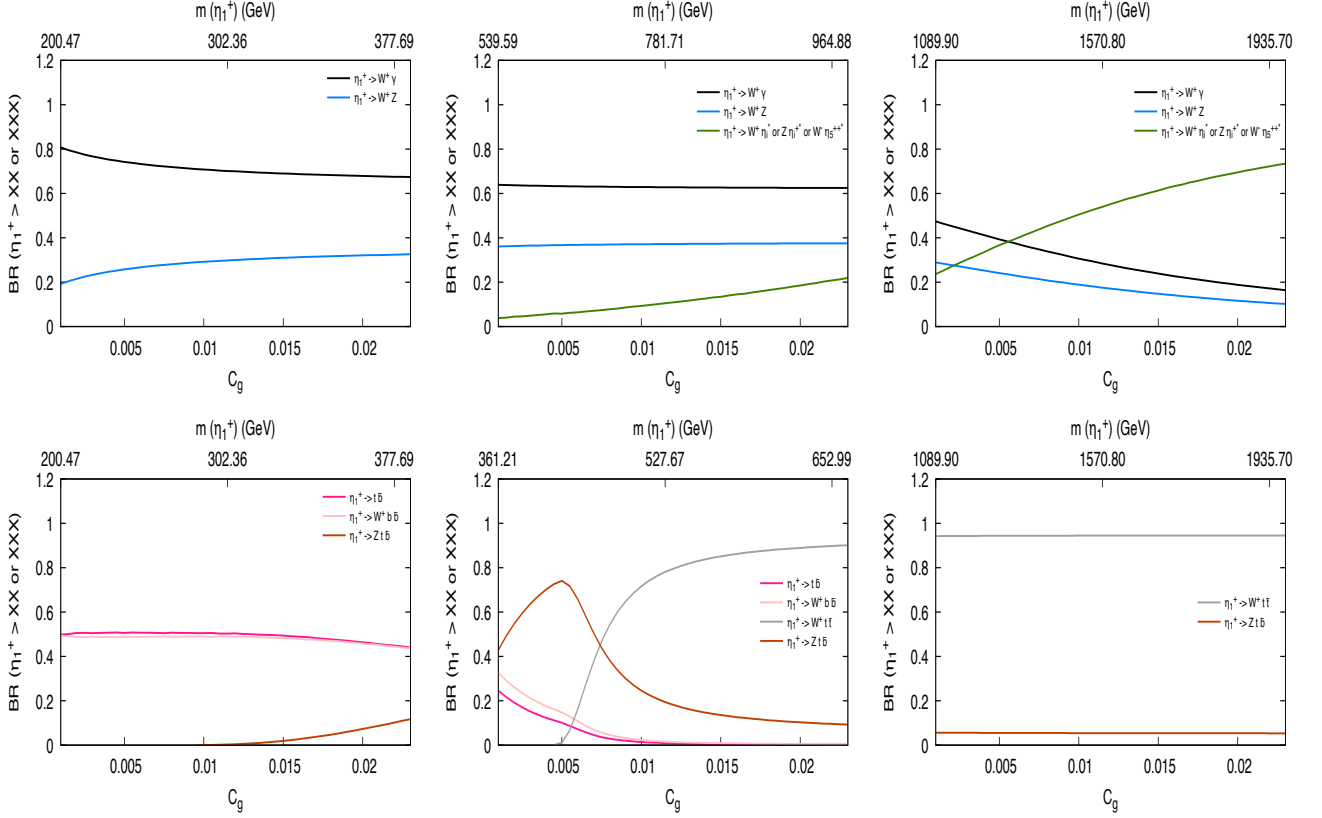


Figure 4: Branching ratios of η_1^\pm for the *fermiophobic* scenario (top panel) and the *fermiophilic* scenario (bottom panel) at $f : 1$ TeV (left), 2.5 TeV (1.7 TeV for *fermiophilic*) (middle) and 5 TeV (right).

We discuss the *fermiophilic* decays of η_1^\pm , now. The dominating decay modes at $f = 1$ TeV are,

$$\eta_1^\pm \rightarrow tb, \quad (39)$$

$$\eta_1^\pm \rightarrow W^\pm \eta_i^* \rightarrow W^\pm bb. \quad (40)$$

The branching ratios are shown in Figure:4 (bottom left). Unlike the case of η_2^\pm , here, the final state $W^\pm bb$ gets negligible contribution from the process with SM quark as the mediator. This is because the coupling $\eta_1^\pm tb$ is suppressed (see Table:3). Further, these decays are dominant over the *fermiophobic* scenario decays to the gauge bosons. Three body decays via off-shell $\eta_5^{\pm\pm}$ are absent since $\eta_5^{\pm\pm}$ does not couple directly to the fermions.

In Figure:4 (bottom middle), we have plotted the branching ratios for $f = 1.7$ TeV⁶. In a very small region of mass range,

$$\eta_1^\pm \rightarrow Z \eta_2^{\pm*} \rightarrow Z t \bar{b} \quad (41)$$

dominates, due to the increased phase space for this decay. With further increase in the mass of η_1^\pm , the process

$$\eta_1^\pm \rightarrow W^\pm \eta_i^* \rightarrow W^\pm t \bar{t} \quad (42)$$

⁶Unlike other pNGB scalar plots, we choose $f = 1.7$ here for better depiction of the variation in branching ratios for intermediate masses.

takes over and dominates its branching ratio, especially at $f = 5$ TeV (Figure:4, bottom right). The absence of decays to any on-shell pNGB scalars is very significant while observing the signatures of η_1^\pm and η_2^\pm at the collider experiments.

4.4 Branching Ratios of the Singlet Neutral scalar, η

The branching ratios of the neutral pNGB scalars are also very interesting which we discuss next. The branching ratios for the singlet scalar, η , are plotted in Figure:5, for the *fermiophobic* scenario (top panel) and the *fermiophilic* scenario (bottom panel). Earlier, we discussed that the singlet scalar η

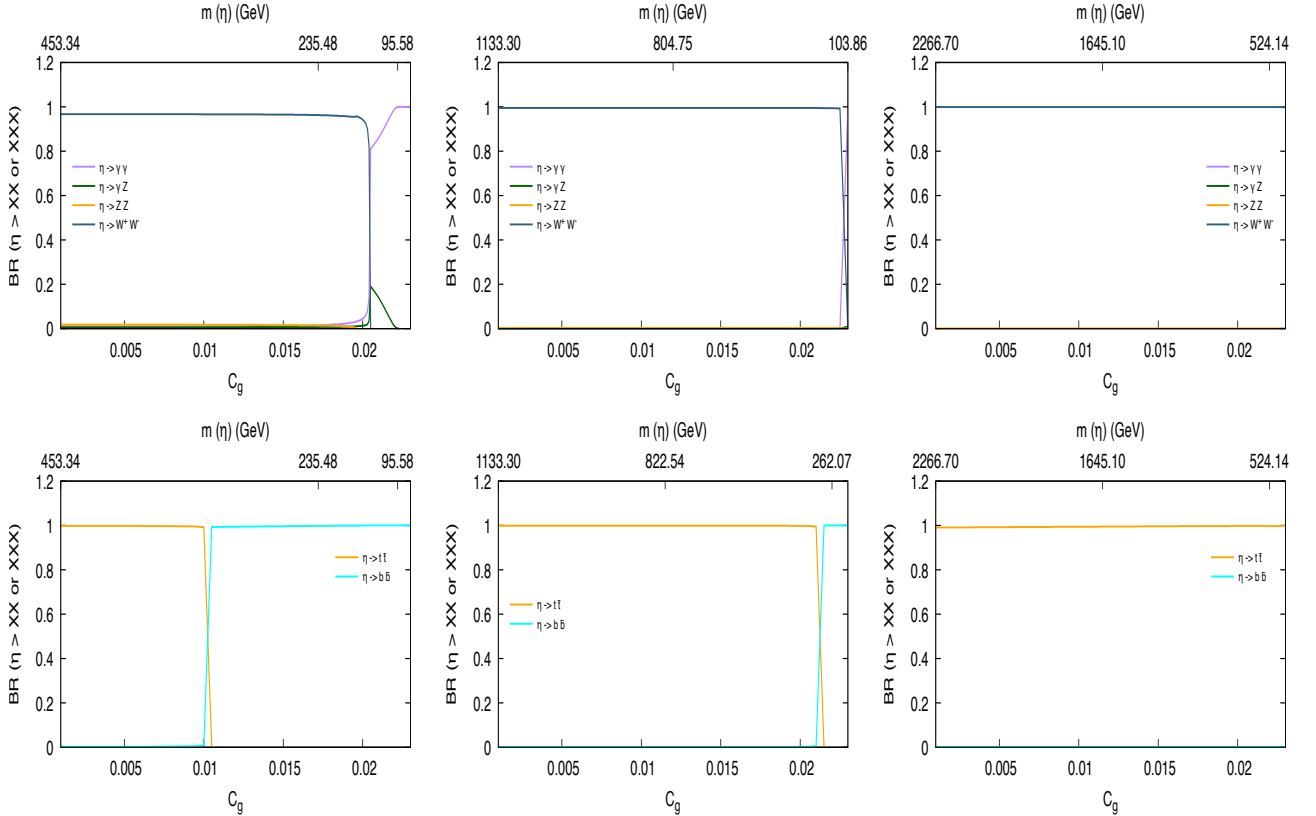


Figure 5: Branching ratios of the singlet scalar η for the *fermiophobic* scenario (top panel) and the *fermiophilic* scenario (bottom panel) at f : 1 TeV (left), 2.5 TeV (middle) and 5 TeV (right).

couple to the gauge bosons but it does not have couplings to any other pNGB scalars. Hence, the decay modes of this neutral scalar, in the *fermiophobic* scenario, are:

$$\eta \rightarrow \gamma Z, \gamma\gamma, ZZ, W^+W^-,$$

as shown in Figure:5 (top panel). The dominating decay mode is W^+W^- , for most of the parameter space. However, towards the upper limit of C_g *i.e.*, when the mass of η is small, $\gamma\gamma$ becomes the dominating decay mode. In the *fermiophilic* scenario *i.e.*, Figure:5 (bottom panel), the major decay modes are

$$\eta \rightarrow bb, tt. \quad (43)$$

The preferential decay to tt at small values of C_g and large values of f may be easily understood from the dependence of η mass on these parameters, as depicted on the parallel x-axis of the plots. As

for the cases of other pNGB scalars, here as well, decays to the gauge bosons are suppressed in the *fermiophilic* scenario.

4.5 Branching Ratios of η_2

The decays of the neutral scalar, η_2 , are shown in Figure:5, for the *fermiophobic* scenario (top panel) and the *fermiophilic* scenario (bottom panel). We, first, discuss the *fermiophobic* scenario (Figure:5,

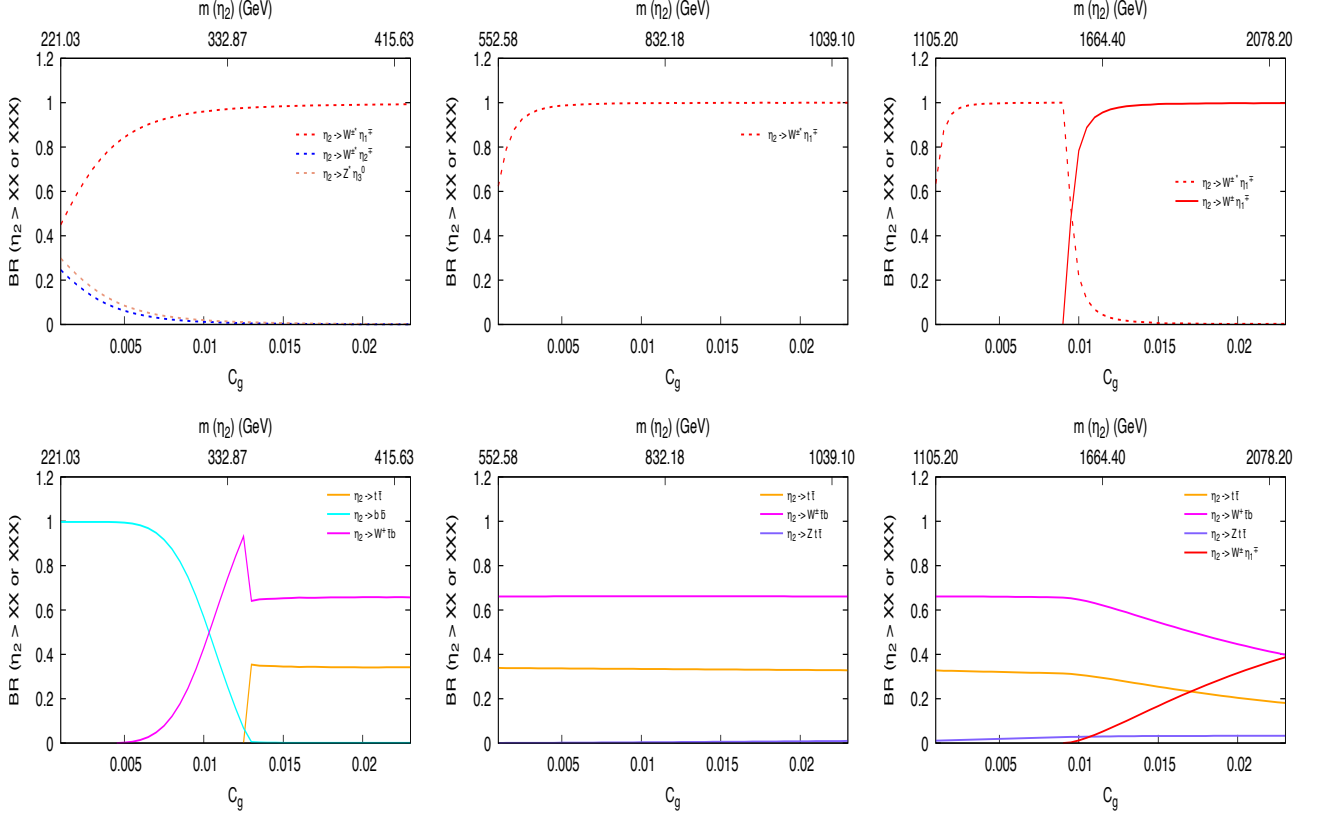


Figure 6: Branching ratios of the singlet scalar η_2 for the *fermiophobic* scenario (top panel) and *fermiophilic* scenario (bottom panel) at f : 1 TeV (left), 2.5 TeV (middle) and 5 TeV (right).

top panel). Considering the mass-hierarchy among the pNGB scalars, the neutral scalar, η_2 , decays to lighter pNGB scalars. At small masses, only three body decays via off-shell W/Z are possible *i.e.*,

$$\eta_2 \rightarrow W^{\pm*} \eta_i^\pm \rightarrow (l\nu) \eta_i^\pm, (qq) \eta_i^\pm, \quad (44)$$

$$\eta_2 \rightarrow Z^* \eta_3^0 \rightarrow (ll)(qq) \eta_3^0. \quad (45)$$

These are the dominating modes at $f = 1$ and 2.5 TeV, with the branching ratio for $\eta_2 \rightarrow W^{\pm*} \eta_1^\pm$ being larger due to large mass-splitting between η_2 and η_1 . The decays to the gauge bosons *viz.*,

$$\eta_2 \rightarrow \gamma Z, \gamma\gamma, ZZ, W^\pm W^\pm \quad (46)$$

are suppressed. At $f = 5$ TeV, due to the increased phase space, on-shell decay $\eta_2 \rightarrow W^\pm \eta_1^\pm$ dominates when $C_g \geq 0.01$.

In the *fermiophilic* scenario (Figure:5, bottom panel), at small masses, the following decays to SM fermions dominate,

$$\eta_2 \rightarrow b\bar{b}, \quad (47)$$

$$\eta_2 \rightarrow t\bar{t}, \quad (48)$$

$$\eta_2 \rightarrow W^\pm \eta_i^{\pm*} \rightarrow W^\pm tb. \quad (49)$$

where $\eta_2 \rightarrow b\bar{b}$ is dominant when enough phase-space is not available for the other decay modes (see Figure:5, bottom left and middle).

At large f , however, the coupling of η_i^\pm to the SM fermions decreases. Hence, the on-shell decay mode $\eta_2 \rightarrow W^\pm \eta_1^\pm$ becomes the dominant decay channel, (see Figure:5, bottom right).

4.6 Branching Ratios of η_1

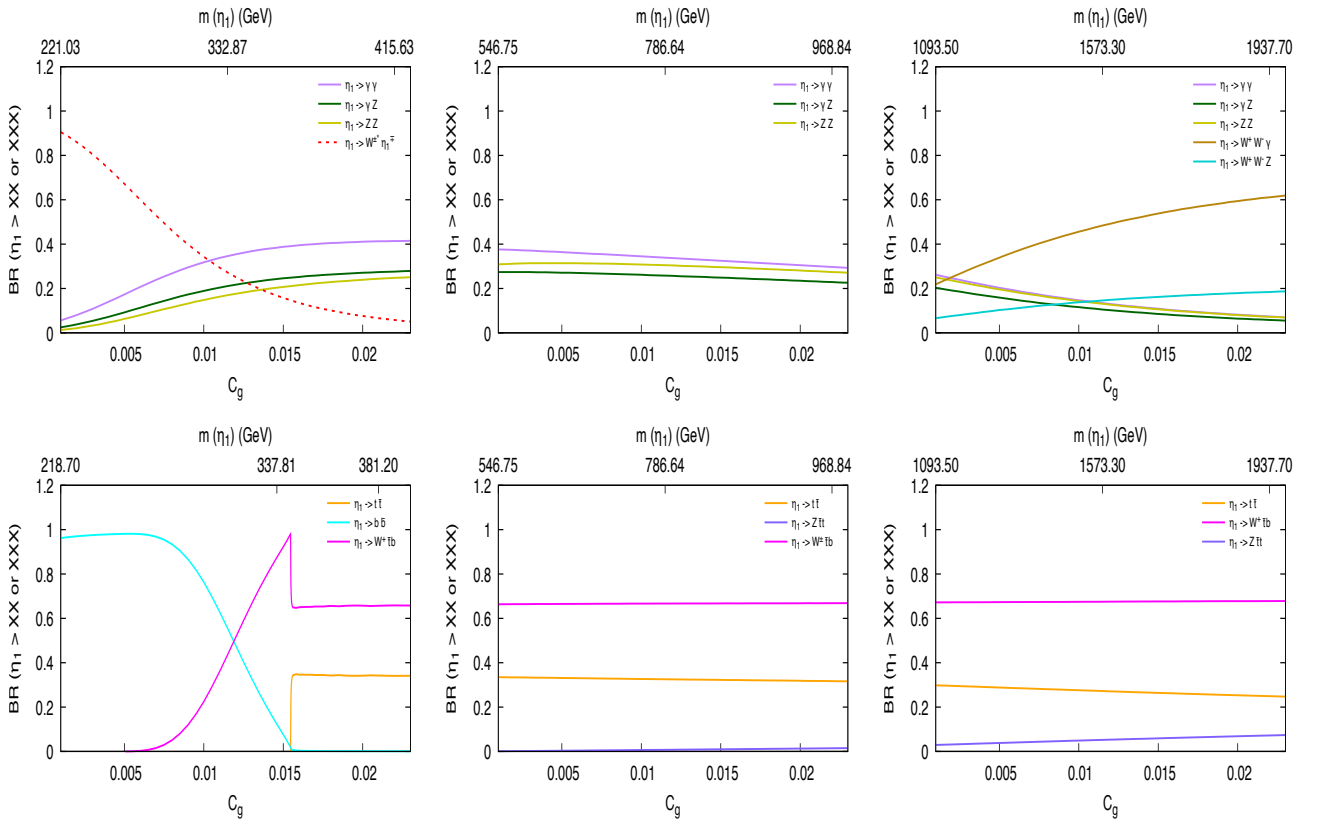


Figure 7: Branching ratios of the singlet scalar η_1 for the *fermiophobic* scenario (top panel) and *fermiophilic* scenario (bottom panel) at f : 1 TeV (left), 2.5 TeV (middle) and 5 TeV (right).

Analogous to the case of charged scalars, the neutral scalar, η_1 , exhibits a completely different behaviour than η_2 , *vis-à-vis*, η_1^\pm and η_2^\pm . We depict the branching ratios for the *fermiophobic* scenario in Figure:7 (top panel). Considering the mass-hierarchy and mass-splittings among the pNGB's, the only decay of η_1 to another pNGB scalar is to η_1^\pm , accompanied by off-shell W boson *i.e.*,

$$\eta_1 \rightarrow W^{\pm*} \eta_1^\pm \rightarrow (l\nu)\eta_1^\pm, (qq)\eta_1^\pm. \quad (50)$$

This decay mode dominates at very small masses only because the small mass-splitting between η_1 and η_1^\pm further diminishes with increase in f . As the mass increases, the dominant contribution comes from the decays to the gauge bosons, mainly from $\gamma\gamma$ (Figure:7, top left and middle). At further larger f (5 TeV), the decays to three gauge bosons dominate *i.e.*,

$$\eta_1 \rightarrow W^+W^-\gamma, W^+W^-Z \quad (51)$$

as shown in Figure:7 (top right). It is important to mention here that unlike Equation:36, these three-body decays mainly proceed via gauge boson propagators. The reason is that due to mixing, η_1 is feebly coupled to other pNGB's and therefore, its coupling to gauge bosons is relatively enhanced.

In the *fermiophilic* scenario, the branching ratios of η_1 are almost similar to η_2 with the exception that at large f , the on-shell decay $\eta_1 \rightarrow W^\pm\eta_1^\pm$ is not possible due to the very small mass difference among the pNGB scalars.

4.7 Branching Ratios of η_3^0

We, now, discuss the branching ratios of the CP-even scalar, η_3^0 . We start with the *fermiophobic* scenario (Figure:8, top panel). The neutral pNGB, η_3^0 , does not decay to two gauge bosons. However, it couples to other pNGB's and one gauge boson. The mass of η_3^0 is close to that of η_2, η_2^\pm and $\eta_5^{\pm\pm}$ and therefore, can only decay to η_1 and η_1^\pm . At small masses ($f = 1$ and 2.5 TeV), however, the dominating decays are via off-shell gauge bosons resulting into three-body decays,

$$\eta_3^0 \rightarrow W^{\pm*}\eta_i^\mp \rightarrow (l\nu)\eta_i^\mp, (qq)\eta_i^\mp, \quad (52)$$

$$\eta_3^0 \rightarrow Z^{\pm*}\eta_i \rightarrow (ll)\eta_i, (qq)\eta_i. \quad (53)$$

For most of the parameter space, these decay modes dominate ((Figure:8, top left and middle). At large f ($f = 5$ TeV), however, phase space becomes available for decays into pNGB's and on-shell gauge bosons and soon, they come to dominate (Figure:8, top right).

$$\eta_3^0 \rightarrow W^\pm\eta_1^\pm, \quad (54)$$

$$\eta_3^0 \rightarrow Z\eta_1. \quad (55)$$

The branching ratios in the *fermiophilic* case are shown in Figure:8 (bottom panel). The decay patterns are similar to the cases of η_2^\pm and η_2 , where decays to SM fermions dominate at small f while at large f , due to reduced coupling to fermions, on-shell decays to lighter pNGB and gauge boson dominates⁷. The only exception is that, unlike other pNGB's, η_3^0 decays to on-shell η_1 , accompanied by a Z boson.

5 Collider Signatures of the Exotic scalars

We have observed that the decay modes of the charged and the neutral pNGB scalars are very different in the *fermiophilic* and *fermiophobic* scenarios. Working in the mass-basis, we derived the masses and mixings of the pNGB's, as a function of the model parameters, f and C_g . The mass-spectrum and the mixings, parameterised by the mixing angles, κ_+ and κ_0 , critically affect the branching ratios of the scalars. The decay modes of the pNGB scalars along with possible collider signatures were also

⁷In case of η_1 , decay to another on-shell pNGB is not possible due to its bra or its small mass

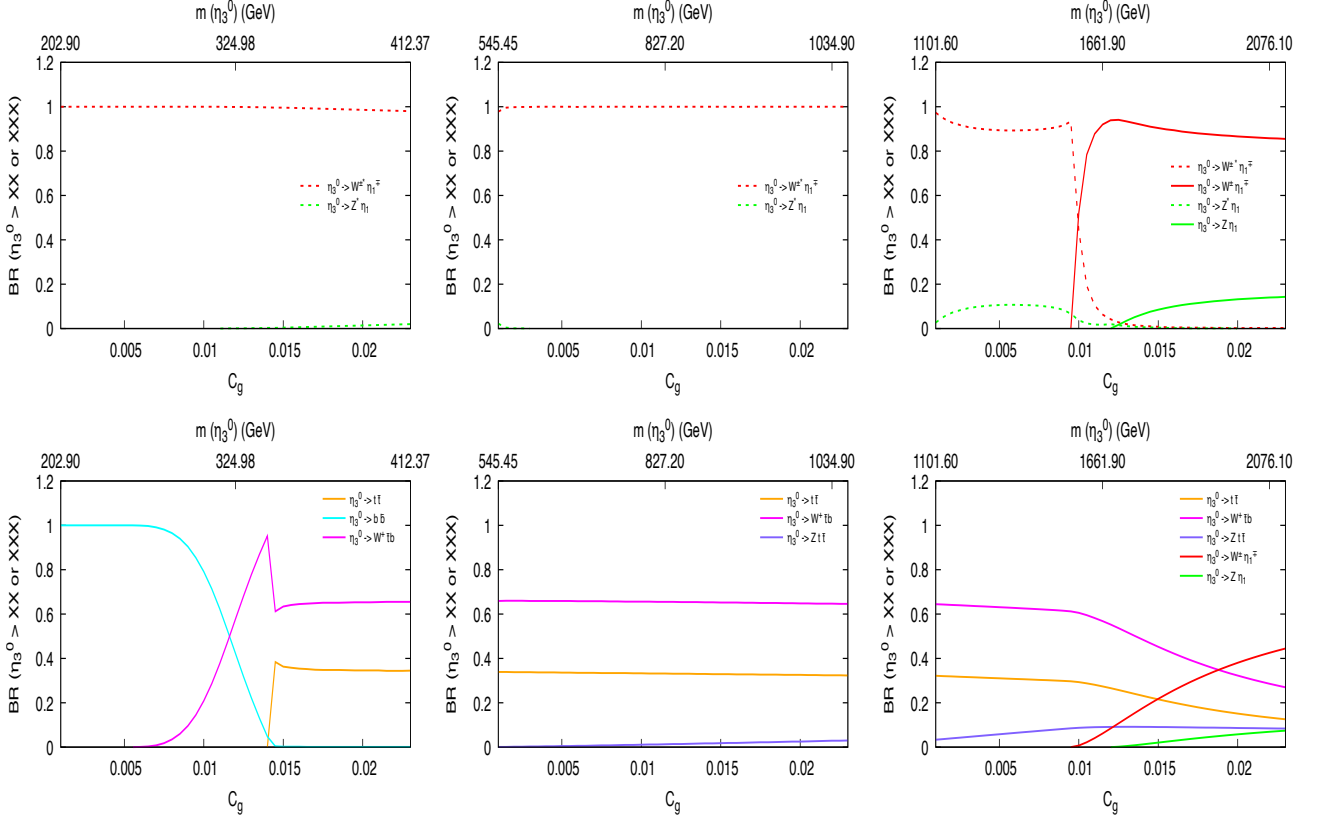


Figure 8: *fermiophobic* decay modes of the neutral scalars as a function of the model parameter C_g at $f = 1, 2.5$ and 5 TeV (left, middle and right).

discussed in [21]. There, particular emphasis was given on the three body decay modes involving off-shell gauge bosons in the intermediate state. In this paper, we have found that the pNGB scalars can decay into an on-shell gauge boson in both *fermiophilic* and *fermiophobic* scenarios. We have observed this in the decays of $\eta_5^{\pm\pm}$, η_2^\pm , η_2 and η_3^0 . In this section, we focus on the charged scalars.

In Table 5, we show some of the branching ratios of these charged scalars in the *fermiophobic* case. These decay modes lead to final states rich in gauge bosons. Depending upon the decays of the W

$\text{BR}(\eta_5^{\pm\pm} \rightarrow W^\pm \eta_1^\pm \rightarrow W^\pm W^\pm Z)$	0.3
$\text{BR}(\eta_2^\pm \rightarrow W^\pm \eta_1 \rightarrow W^\pm W^+ W^- \gamma)$	0.36

Table 5: Approximate branching ratios when the charged pNGB scalars decay to an on-shell gauge boson and another on-shell pNGB scalar. We fix $f = 5$ TeV and masses are greater than 1 TeV.

and Z bosons, multi-lepton and/or multi-jet final states are possible.

In Fig 9, we plot the production cross-section of the charged pNGB scalars at the 14 TeV LHC. Masses of the scalars are represented as a function of C_g while the value of f is fixed at 1 TeV. At this value of f , the masses of the scalars are below 500 GeV. The decays that we are concerned about occur mostly at $f = 5$ TeV, $C_g = 0.01$, placing all pNGB scalars near 1 TeV. For TeV scale charged scalars, the cross-section at the LHC is estimated to be $\sim \mathcal{O}(1)$ fb or even smaller.

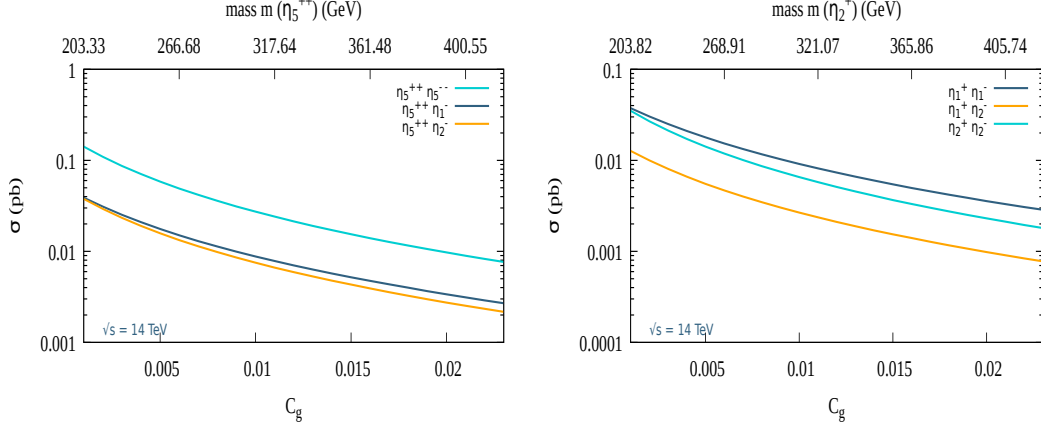


Figure 9: Production cross-sections of the charged scalars at the LHC 14 TeV with $f = 1$ TeV.

For the multijet signatures, lepton colliders will be more effective because of their cleaner environment. Future lepton colliders [34–36] provide the opportunity to detect exotic particles at energies below the TeV scale. However, these above mentioned signatures occur when the pNGB masses are ~ 1 TeV. Hence, muon collider [32, 33, 37, 38] will be a great alternative in order to achieve higher masses of the pNGB scalars. The advantage of the muon collider is twofold. Contrary to the circular colliders, a muon collider suppresses the loss of energy due to synchrotron radiation because of the heavier mass of muon, thereby, making both high energy as well as high luminosity achievable. We plot the production cross-section of the pNGB scalars at the muon collider in Fig:10. One may note that the

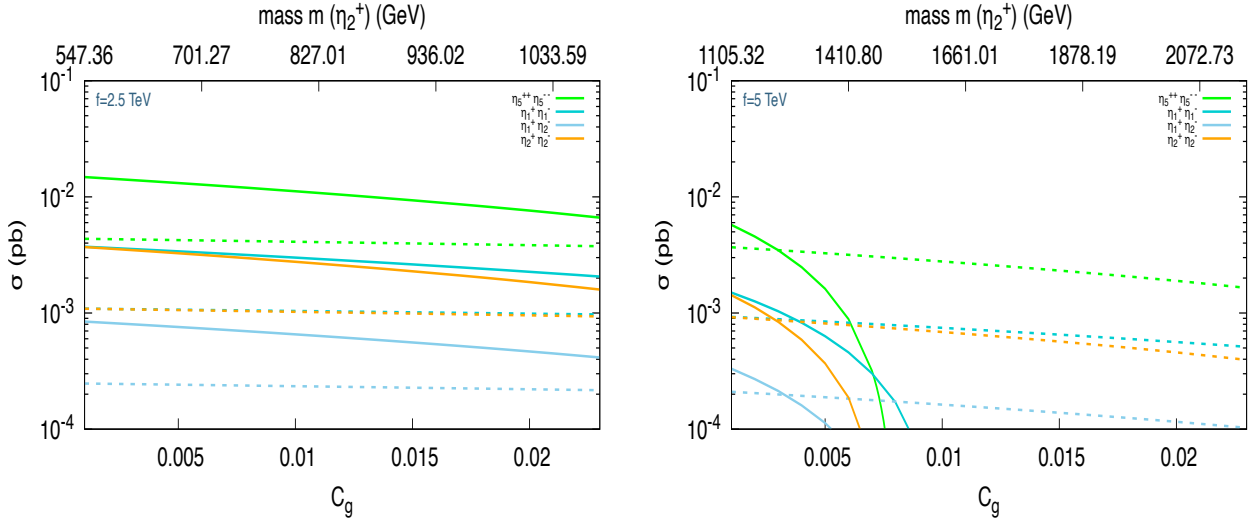


Figure 10: Production cross-sections of the pNGB scalars at $\mu^+\mu^-$ collider for $\sqrt{s} = 3$ TeV (solid lines) and $\sqrt{s} = 6$ TeV (dashed lines).

production cross-section of the singly charged scalars are different due to difference in their gauge couplings. We have also seen that the decay modes are very different for these two pNGB scalars. Both these factors will attribute to the detection of the singly charged scalars in the muon collider

experiments. In addition to the above *fermiophobic* case, the *fermiophilic* scenario also offers some unique signatures. We will discuss these in an upcoming study.

6 Conclusion

Key unanswered questions that remain after the discovery of Higgs are about the Higgs' fundamental versus composite nature, its unprotected mass from high-scale quantum corrections, and the absence of a dynamical electroweak symmetry breaking (EWSB) mechanism in the SM. Composite Higgs models address these issues by introducing a TeV-scale strongly interacting sector where the Higgs emerges as a pseudo-Nambu Goldstone boson (pNGB) from spontaneous symmetry breaking. In the non-minimal composite model based on $SU(5)/SO(5)$ framework, resembling the Georgi-Machacek model at low energies, features a rich scalar sector. The *fermiophilic* and *fermiophobic* decay channels for pNGBs are influenced by fermion embedding choices in $SU(5)/SU(5)$ representations.

Recent studies have examined the *fermiophilic* and *fermiophobic* scenarios, analyzing collider signatures and the LHC constraints under simplified assumptions with fixed compositeness scale f and scalar masses. However, the compositeness scale f (varied from 1–5 TeV) is intrinsically linked to fine-tuning, which depends on fermion representation choices. In this work, we have shown that the masses and mixings of pNGB scalars, as functions of f and gauge-loop parameter C_g , have a key influence on the branching ratios of the pNGB scalars. Unlike the prior works, this study incorporates mixing between gauge and mass eigenstates, deriving couplings in terms of the mixing angles, which influences the scalar phenomenology.

In this paper we have studied the *fermiophilic* and *fermiophobic* couplings, in detail, for the full scalar spectrum, where, the scalar masses range from $\sim (200 - 2000)$ GeV. We find that the decay pattern of the scalars are very distinct at different masses. The on-shell and off-shell decay modes are highly dependent on the mass differences among the pNGB scalars, which is calculated explicitly in terms of the model parameters. We show that the branching ratios of the two singly charged scalars, η_1^\pm and η_2^\pm are very different. For the *fermiophobic* scenario, at small masses, both the scalars decay to the gauge bosons but at large masses, their decay patterns change. The heavier η_2^\pm decays to another on-shell pNGB scalar, accompanied by an off-shell or on-shell gauge boson. On the other hand, the scalar, η_1^\pm , due to its small mass-splitting with the other pNGB's, cannot decay to an on-shell pNGB scalar. Instead, it prefers to decay to the gauge bosons or on-shell gauge bosons with off-shell pNGB scalars, the latter eventually leading to three gauge bosons. For the *fermiophilic* scenario, η_2^\pm decays to tb or $W^\pm bb$ at small masses and on-shell pNGB's at large masses. The scalar, η_1^\pm , instead, prefers decaying to tb and $W^\pm bb$ at small masses, Ztb at intermediate masses and $W^\pm tt$ at large masses. Thus, at the collider experiments, these singly charged scalars generate distinct signatures. We plan to study these signatures in a follow up work.

Acknowledgments

N.K expresses gratitude to A.M. Anirudhan for his contributions during the initial stages of this project, where he served as the project associate (PA-1) under SRG/2022/000363. N.K. would like to thank Department of Science and Technology and Anusandhan National Research Foundation Government of India for the support from the Startup Research Grant, grant agreement number SRG/2022/000363 and Core Research Grant with grant agreement number CRG/2022/004120.

References

- [1] Robert D. Harrington. Observation of an excess of events in the Higgs boson search in ATLAS. *Nucl. Phys. B Proc. Suppl.*, 234:15–20, 2013.
- [2] Serguei Chatrchyan et al. Observation of a New Boson at a Mass of 125 GeV with the CMS Experiment at the LHC. *Phys. Lett. B*, 716:30–61, 2012.
- [3] B. Abi et al. Measurement of the Positive Muon Anomalous Magnetic Moment to 0.46 ppm. *Phys. Rev. Lett.*, 126(14):141801, 2021.
- [4] Georges Aad et al. Constraints on the Higgs boson self-coupling from single- and double-Higgs production with the ATLAS detector using pp collisions at $s=13$ TeV. *Phys. Lett. B*, 843:137745, 2023.
- [5] S. Navas et al. Review of particle physics. *Phys. Rev. D*, 110(3):030001, 2024.
- [6] David B. Kaplan and Howard Georgi. SU(2) x U(1) Breaking by Vacuum Misalignment. *Phys. Lett. B*, 136:183–186, 1984.
- [7] Michael J. Dugan, Howard Georgi, and David B. Kaplan. Anatomy of a Composite Higgs Model. *Nucl. Phys. B*, 254:299–326, 1985.
- [8] Roberto Contino. The Higgs as a Composite Nambu-Goldstone Boson. In *Theoretical Advanced Study Institute in Elementary Particle Physics: Physics of the Large and the Small*, pages 235–306, 2011.
- [9] Giuliano Panico and Andrea Wulzer. *The Composite Nambu-Goldstone Higgs*, volume 913. Springer, 2016.
- [10] Kaustubh Agashe, Roberto Contino, and Alex Pomarol. The Minimal composite Higgs model. *Nucl. Phys. B*, 719:165–187, 2005.
- [11] Giuliano Panico and Andrea Wulzer. The Discrete Composite Higgs Model. *JHEP*, 09:135, 2011.
- [12] Oleksii Matsedonskyi, Giuliano Panico, and Andrea Wulzer. Light Top Partners for a Light Composite Higgs. *JHEP*, 01:164, 2013.
- [13] Ed Bennett, Deog Ki Hong, Jong-Wan Lee, C. J. David Lin, Biagio Lucini, Maurizio Piai, and Davide Vadicchino. Sp(4) gauge theory on the lattice: towards SU(4)/Sp(4) composite Higgs (and beyond). *JHEP*, 03:185, 2018.
- [14] Avik Banerjee, Gautam Bhattacharyya, and Tirtha Sankar Ray. Improving Fine-tuning in Composite Higgs Models. *Phys. Rev. D*, 96(3):035040, 2017.
- [15] Avik Banerjee, Gautam Bhattacharyya, Nilanjana Kumar, and Tirtha Sankar Ray. Constraining Composite Higgs Models using LHC data. *JHEP*, 03:062, 2018.
- [16] Teng Ma and Giacomo Cacciapaglia. Fundamental Composite 2HDM: SU(N) with 4 flavours. *JHEP*, 03:211, 2016.
- [17] Haiying Cai and Giacomo Cacciapaglia. Singlet dark matter in the SU(6)/SO(6) composite Higgs model. *Phys. Rev. D*, 103(5):055002, 2021.

- [18] Sebastian Bruggisser, Benedict Von Harling, Oleksii Matsedonskyi, and Géraldine Servant. Baryon Asymmetry from a Composite Higgs Boson. *Phys. Rev. Lett.*, 121(13):131801, 2018.
- [19] A. Doff and Clarissa Siqueira. Composite Higgs Models, Technicolor and The Muon Anomalous Magnetic Moment. *Phys. Lett. B*, 754:294–301, 2016.
- [20] Georges Aad et al. Search for doubly and singly charged Higgs bosons decaying into vector bosons in multi-lepton final states with the ATLAS detector using proton-proton collisions at $\sqrt{s} = 13$ TeV. *JHEP*, 06:146, 2021.
- [21] G. Cacciapaglia, T. Flacke, M. Kunkel, W. Porod, and L. Schwarze. Exploring extended Higgs sectors via pair production at the LHC. *JHEP*, 12:087, 2022.
- [22] Alessandro Agugliaro, Giacomo Cacciapaglia, Aldo Deandrea, and Stefania De Curtis. Vacuum misalignment and pattern of scalar masses in the SU(5)/SO(5) composite Higgs model. *JHEP*, 02:089, 2019.
- [23] Gabriele Ferretti. UV Completions of Partial Compositeness: The Case for a SU(4) Gauge Group. *JHEP*, 06:142, 2014.
- [24] Christoph Englert, Emanuele Re, and Michael Spannowsky. Pinning down Higgs triplets at the LHC. *Phys. Rev. D*, 88:035024, 2013.
- [25] Avik Banerjee, Gautam Bhattacharyya, and Nilanjana Kumar. Impact of Yukawa-like dimension-five operators on the Georgi-Machacek model. *Phys. Rev. D*, 99(3):035028, 2019.
- [26] Robyn Campbell, Stephen Godfrey, Heather E. Logan, and Alexandre Poulin. Real singlet scalar dark matter extension of the Georgi-Machacek model. *Phys. Rev. D*, 95(1):016005, 2017.
- [27] Gabriele Ferretti. Gauge theories of Partial Compositeness: Scenarios for Run-II of the LHC. *JHEP*, 06:107, 2016.
- [28] Nicolas Bizot, Giacomo Cacciapaglia, and Thomas Flacke. Common exotic decays of top partners. *JHEP*, 06:065, 2018.
- [29] Avik Banerjee et al. Phenomenological aspects of composite Higgs scenarios: exotic scalars and vector-like quarks. 3 2022.
- [30] James Barnard, Daniel Murnane, Martin White, and Anthony G. Williams. Constraining fine tuning in Composite Higgs Models with partially composite leptons. *JHEP*, 09:049, 2017.
- [31] Nima Arkani-Hamed, Tao Han, Michelangelo Mangano, and Lian-Tao Wang. Physics opportunities of a 100 TeV proton–proton collider. *Phys. Rept.*, 652:1–49, 2016.
- [32] Jean Pierre Delahaye, Marcella Diemoz, Ken Long, Bruno Mansoulié, Nadia Pastrone, Lenny Rivkin, Daniel Schulte, Alexander Skrinsky, and Andrea Wulzer. Muon Colliders. 1 2019.
- [33] Tao Han, Shuailong Li, Shufang Su, Wei Su, and Yongcheng Wu. BSM Higgs Production at a Muon Collider. In *Snowmass 2021*, 5 2022.
- [34] Nilanjana Kumar. Unconventional Searches for Exotic Particles at Future Lepton Colliders. *EPJ Web Conf.*, 315:01034, 2024.
- [35] Strahinja Lukić. Physics highlights at ILC and CLIC. In *12th International School-Seminar on The Actual Problems of Microworld Physics*, volume 1, pages 39–53, 2015.

- [36] Alexander Aryshev et al. The International Linear Collider: Report to Snowmass 2021. 3 2022.
- [37] Carlotta Accettura et al. Interim report for the International Muon Collider Collaboration (IMCC). *CERN Yellow Rep. Monogr.*, 2/2024:176, 2024.
- [38] Carlotta Accettura et al. Towards a muon collider. *Eur. Phys. J. C*, 83(9):864, 2023. [Erratum: *Eur.Phys.J.C* 84, 36 (2024)].